Inorganic Chemistry

pubs.acs.org/IC Article

Synthesis and Reactivity Studies of a Series of Nickel(II) Arylchalcogenolates

Lauren L. Cordeiro, Olga Dmitrenko, Glenn P. A. Yap, and Charles G. Riordan*

Cite This: *Inorg. Chem.* 2021, 60, 6327−6338 Read Online

ABSTRACT: Two series of high-spin nickel complexes, $[Tp^{Ph,Me}]Ni(EAr)$ (E = O, Se, Te; Ar = C_6H_5) and $[Tp^{Ph,Me}]Ni(SeC_6H_4\text{-}4\text{-}X)$ (X = H, Cl, Me, OMe), were prepared by metathetical reaction of the nickel(II) halide precursor with sodium salts of the corresponding chalcogen, NaEAr. X-ray crystallographic characterization and spectroscopic studies have established the geometric and electronic structures of these complexes. The observed spectroscopic and structural characteristics reveal distinct trends in accordance with the variation of the identity of the arylchalcogenolate and *para* substituent. Reaction of the $[Tp^{Ph,Me}]Ni(EAr)$ complexes with methyl iodide proceeded readily, producing the corresponding methylarylchalcogen and $[Tp^{Ph,Me}]NiI$. A kinetic and computational analysis of the reaction of $[Tp^{Ph,Me}]Ni(SeC_6H_5)$ with MeI supports that the electrophilic alkylation reactions occur via an associative mechanism via a classical S_N2 transition state.

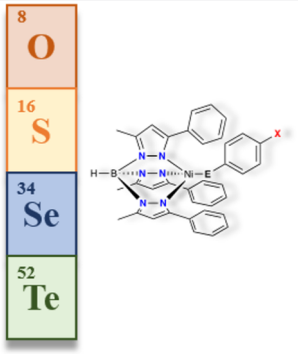

■ INTRODUCTION

Metal complexes containing organochalcogenide ligands comprise the class of compounds referred to collectively as metal chalcogenolates. These materials have applications in catalysis,[1−4] electronic materials,[5−8] medicine,[9] and biomimetic chemistry. There are numerous benefits to the development of new metal chalcogenolate complexes. An investigation of the geometric and electronic structures of these complexes leads to a greater understanding of the effects that chalcogen atom variation has on the nature of the metal−ligand bonding. This applies especially to the generation of isostructural metal chalcogenolates, where relevant differences among the chalcogens can be readily observed.

Prior studies have been devoted primarily to investigating the reactivity of metal−thiolate complexes due to their prevalence in metalloprotein active sites.[10,11] Examples include blue copper proteins,[12] cytochrome P450,[13] nickel superoxide dismutase,[14] Fe/Ni-hydrogenase,[15] methyl coenzyme M reductase,[16] acetyl coenzyme A synthase,[17] and zinc-dependent methyltransferases.[18] These metalloproteins consist of a diverse array of metals that support a variety of protein and enzymatic functions. Pertinent to this study is the key function of zinc-containing macromolecules, which is the promotion of biological alkyl group transfer. This typically occurs in the manner of alkylation of a zinc−cysteine thiolate residue, as seen in the reactivity of the Ada DNA repair protein.[19,20] Several synthetic model systems have been developed to elucidate the mechanism by which this alkyl transfer reaction occurs.[21−24] Efforts have been directed primarily toward identifying the active nucleophile in the reaction. It has been proposed that alkylation can occur by two distinct mechanisms, both of which involve alkylation at the nucleophilic thiolate. One path is an associative mechanism, wherein alkylation takes place at the metal-bound thiolate. The other is a dissociative mechanism involving alkylation at the "free" thiolate. The possible associative and dissociative pathways are depicted in Scheme 1. Although it is not drawn explicitly, the

Scheme 1

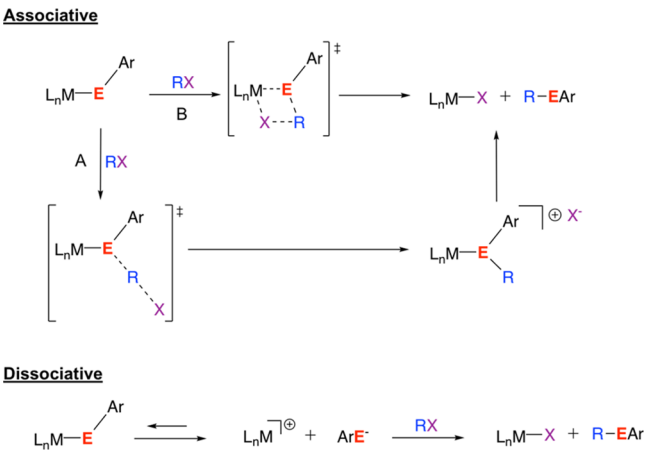

Received: January 8, 2021
Published: April 14, 2021

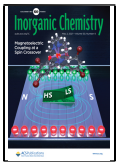

https://doi.org/10.1021/acs.inorgchem.1c00066
Inorg. Chem. 2021, 60, 6327−6338

dissociative path can involve solvent stabilization: e.g., of the dissociated metal species as noted by Wilker and Lippard.[21] Both associative and dissociative mechanisms have been assigned as operative in a variety of reactivity studies with metal−thiolates.

In the interest of providing a comprehensive examination of electrophilic alkylation for complexes of the type M-ER, herein are presented the synthesis, characterization, and reactivity of a series of arylchalcogenolate nickel complexes, [$Tp^{Ph,Me}$]Ni(EAr). The $Tp^{Ph,Me}$ ligand was found to support the series of [$Tp^{Ph,Me}$]Ni(EAr) complexes, including those for E = O, Se, Te and Ar = C_6H_5, as well as the arylselenolate series [$Tp^{Ph,Me}$]Ni(SeC_6H_4-4-X) (X = H, Cl, Me, OMe) designed to uncover the impact of the electronic effects of the aryl selenolates on alkylation reactions. The development of the complete arylchalcogenolate series has presented an opportunity to explore the reactivity of these complexes. In an effort to elucidate the nature of the electrophilic alkylation mechanism for nickel(II) arylchalcogenolates, a combination of experimental methods and complementary density functional theory (DFT) results is presented.

■ EXPERIMENTAL SECTION

General Considerations. All reactions were performed under an inert atmosphere of nitrogen either in a Vacuum Atmospheres glovebox or by using standard Schlenk techniques. All reagents purchased from commercial sources were used as received. *para*-Substituted aromatic diselenide reagents, if not commercially available, were prepared according to literature methods.[25] Sodium salts of chalcogenides were prepared through addition of either Na metal or $NaBH_4$ to a solution of the corresponding dichalcogenide.[26]

^{1}H NMR spectra were recorded on a Bruker AVIII 400 MHz NMR spectrometer, and chemical shifts (δ) were referenced to the residual protons in the deuterated solvents. Electronic absorption spectra were recorded on a Varian Cary 50 spectrophotometer. Chemical kinetic reactions monitored through UV−vis were temperature-controlled using a Unisoku CoolSpek UV Cryostat. Solid-state IR samples were prepared as KBr pellets, and FT-IR spectra were recorded on a Nicolet Magna-IR 560 spectrophotometer with a resolution of 4 cm^{-1}. The Evans method was used to obtain solution magnetic moments in toluene-d_8, at 298 K.[27] High-resolution mass spectra were recorded using a Waters GCT mass spectrometer with a liquid field desorption ionization (LIFDI) source. Elemental analyses were obtained from Robertson Microlit (Ledgewood, NJ).

Synthesis of [$Tp^{Ph,Me}$]Ni(OC_6H_5). To a solution of [$Tp^{Ph,Me}$]NiI (100 mg, 0.15 mmol) in toluene (15 mL) was added a slurry of $NaOC_6H_5$ (26 mg, 0.22 mmol) in toluene (5 mL). The solution turned from dark red-brown to brown-orange. The reaction mixture was stirred overnight, followed by removal of the solvent under vacuum. The product was recrystallized by vapor diffusion of pentane into a concentrated toluene solution: 64 mg, 67% crystalline yield. UV−vis (THF): λ_{max}, nm (ε, M^{-1} cm^{-1}) 430 (2608), 500 (sh, 1200), 905 (273). ^{1}H NMR (C_6D_6, 400 MHz): δ 74.2 (4-Pz, s, 3H), 37.2 (*m*-Ph, OPh, s, 2H), 16.1 (*o*-Ph, m, 6H), 8.4 (*m*-Ph, m, 6H), 7.1 (*p*-Ph, m, 3H), −1.6 (5-Me, s, 9H), −20.5 (B-*H*, br, 1H), −43.6 (*p*-Ph, OPh, s, 2H), −48.9 (*o*-Ph, OPh, s, 1H). FTIR (KBr; ν, cm^{-1}): 2543 (B−H). Combustion analysis was attempted, but adequate results were not obtained. LIFDI-MS (*m*/*z*): calcd for $C_{36}H_{33}N_6BNiO$, 634.22; found, 634.22. μ_{eff} = 3.04(4) μ_B.

Synthesis of [$Tp^{Ph,Me}$]Ni(SeC_6H_5). To a solution of [$Tp^{Ph,Me}$]NiI (100 mg, 0.15 mmol) in toluene (15 mL) was added a slurry of $NaSeC_6H_5$ (40 mg, 0.22 mmol) in toluene (5 mL). The solution turned from dark red-brown to deep cobalt blue. The reaction mixture was stirred overnight, followed by removal of the solvent under vacuum. The product was recrystallized by vapor diffusion of pentane into a concentrated toluene solution: 82 mg, 79% crystalline yield. UV−vis (THF): λ_{max}, nm (ε, M^{-1} cm^{-1}) 580 (5695), 910 (880). ^{1}H NMR (C_6D_6, 400 MHz): δ 68.8 (4-Pz, s, 3H), 22.3 (*m*-Ph, SePh, s, 2H), 9.6 (*o*-Ph, m, 6H), 7.8 (*m*-Ph, m, 6H), 7.1 (*p*-Ph, m, 3H), 4.9 (5-Me, s, 9H), −8.5 (B-*H*, br, 1H), −23.0 (*o*-Ph, SePh, s, 2H), −29.8 (*p*-Ph, SePh, s, 2H). FTIR (KBr pellet, ν, cm^{-1}): 2545 (B−H). Anal. Calcd for $C_{36}H_{33}N_6BNiSe$: C, 61.93, H, 4.76, N, 12.04. Found: C, 61.90, H, 4.68, N, 12.08. μ_{eff} = 2.80(4) μ_B.

Synthesis of [$Tp^{Ph,Me}$]Ni(SeC_6H_4-4-Cl). To a solution of [$Tp^{Ph,Me}$]NiI (370 mg, 0.55 mmol) in toluene (20 mL) was added a slurry of $NaSeC_6H_4$-4-Cl (181 mg, 0.85 mmol) in toluene (5 mL). The solution turned from dark red-brown to dark violet. The reaction mixture was stirred overnight, followed by removal of the solvent under vacuum. The product was recrystallized by vapor diffusion of pentane into a concentrated toluene solution: 273 mg, 67% crystalline yield. UV−vis (THF): λ_{max}, nm (ε, M^{-1}c m^{-1}) 570 (3188), 910 (579).^{1}H NMR (C_6D_6, 400 MHz): δ 69.8 (4-Pz, s, 3H), 22.3 (*m*-Ph, SePh, s, 2H), 9.2 (*o*-Ph, m, 6H), 7.8 (*m*-Ph, m, 6H), 7.0 (*p*-Ph, m, 3H), 5.2 (5-Me, s, 9H), −8.5 (B-*H*, br, 1H), −22.2 (*o*-Ph, SePh, s, 2H). FTIR (KBr pellet, ν, cm^{-1}): 2537 (B−H). Anal. Calcd for $C_{36}H_{32}N_6BNiSeCl$: C, 59.02, H, 4.40, N, 11.47. Found: C, 58.75, H, 4.19, N, 11.19. μ_{eff} = 2.85(6) μ_B.

Synthesis of [$Tp^{Ph,Me}$]Ni(SeC_6H_4-4-Me). To a solution of [$Tp^{Ph,Me}$]NiI (100 mg, 0.15 mmol) in toluene (20 mL) was added a slurry of $NaSeC_6H_4$-4-Me (44 mg, 0.23 mmol) in toluene (5 mL). The solution turned from dark red-brown to dark blue. The reaction mixture was stirred overnight, followed by removal of the solvent under vacuum. The product was recrystallized by vapor diffusion of pentane into a concentrated toluene solution: 67 mg, 63% crystalline yield. UV−vis (THF): λ_{max}, nm (ε, M^{-1} cm^{-1}) 585 (5353), 935 (915). ^{1}H NMR (C_6D_6, 400 MHz): δ 68.3 (4-Pz, s, 3H), 39.5 (*pMe*-Ph, SePh, s, 3H), 22.3 (*m*-Ph, SePh, s, 2H), 9.6 (*o*-Ph, m, 6H), 7.8 (*m*-Ph, m, 6H), 7.1 (*p*-Ph, m, 3H), 4.8 (5-Me, s, 9H), −8.4 (B-*H*, br, 1H), −23.7 (*o*-Ph, SePh, s, 2H). FTIR (KBr pellet, ν, cm^{-1}): 2534 (B−H). Anal. Calcd for $C_{37}H_{35}N_6BNiSe$: C, 62.40, H, 4.95, N, 11.80. Found: C, 62.19, H, 5.09, N, 11.69. μ_{eff} = 2.85(4) μ_B.

Synthesis of [$Tp^{Ph,Me}$]Ni(SeC_6H_4-4-OMe). To a solution of [$Tp^{Ph,Me}$]NiI (100 mg, 0.15 mmol) in toluene (20 mL) was added a slurry of $NaSeC_6H_4$-4-OMe (48 mg, 0.23 mmol) in toluene (5 mL). The solution turned from dark red-brown to dark blue. The reaction mixture was stirred overnight, followed by removal of the solvent under vacuum. The product was recrystallized by vapor diffusion of pentane into a concentrated toluene solution: 92 mg, 85% crystalline yield. UV−vis (THF): λ_{max}, nm (ε, M^{-1} cm^{-1}) 600 (4165), 935 (877). ^{1}H NMR (C_6D_6, 400 MHz): δ 68.1 (4-Pz, s, 3H), 21.3 (*m*-Ph, SePh, s, 2H), 9.7 (*o*-Ph, m, 6H), 7.8 (*m*-Ph, m, 6H), 7.1 (*p*-Ph, m, 3H), 6.8 (*pOMe*-Ph, SePh, 3H), 4.7 (5-Me, s, 9H), −8.2 (B-*H*, br, 1H), −24.9 (*o*-Ph, SePh, s, 2H). FTIR (KBr pellet, ν, cm^{-1}): 2516 (B−H). Anal. Calcd. for $C_{37}H_{35}N_6BNiSeO$: C, 61.03, H, 4.84, N, 11.54. Found: C, 61.33, H, 4.76, N, 11.59. μ_{eff} = 2.78(2) μ_B.

Synthesis of [$Tp^{Ph,Me}$]Ni(TeC_6H_5). To a solution of [$Tp^{Ph,Me}$]NiI (140 mg, 0.21 mmol) in toluene (20 mL) was added a solution of $NaTeC_6H_5$ (71 mg, 0.31 mmol) in toluene (5 mL). The solution turned from a dark red-brown to a dark teal. The reaction mixture was stirred for 2 h, followed by removal of the solvent under vacuum. Dark green crystals were obtained by diffusion of pentane into an ethyl ether solution: 83 mg, 53% crystalline yield. UV−vis (THF): λ_{max}, nm (ε, M^{-1} cm^{-1}) 440 (800), 670 (2755). ^{1}H NMR (C_6D_6, 400 MHz): δ 66.7 (4-Pz, s, 3H), 19.2 (*m*-Ph, TePh, s, 2H), 8.2 (*o*-Ph, m, 6H), 7.6 (*m*-Ph, m, 6H), 6.9 (*p*-Ph, m, 3H), 6.5 (5-Me, s, 9H), −5.3 (B-*H*, br, 1H), −20.2 (*o*-Ph, TePh, s, 2H), −23.7 (*p*-Ph, TePh, s, 2H). FTIR (KBr, ν/cm^{-1}): 2536 (B−H). Anal. Calcd for $C_{36}H_{33}N_6BNiTe$: C, 57.90, H, 4.45, N, 11.25. Found: C, 58.06, H, 4.88, N, 11.61. μ_{eff} = 2.73(1) μ_B.

Monitoring of the Kinetics of [$Tp^{Ph,Me}$]Ni(EAr) Reacting with MeI. All reaction solutions were prepared under a nitrogen atmosphere. A 5 mL solution of the appropriate [$Tp^{Ph,Me}$]Ni(EAr) complex was prepared and placed into a cuvette that was then sealed with a rubber septum. The reaction kinetics were conducted at 25 °C under pseudo-first-order conditions. Temperatures were maintained using a Unisoku CoolSpek UV Cryostat. Neat methyl iodide was added via a gastight syringe in at least 100-fold excess, ensuring

https://doi.org/10.1021/acs.inorgchem.1c00066
Inorg. Chem. 2021, 60, 6327−6338

Scheme 2

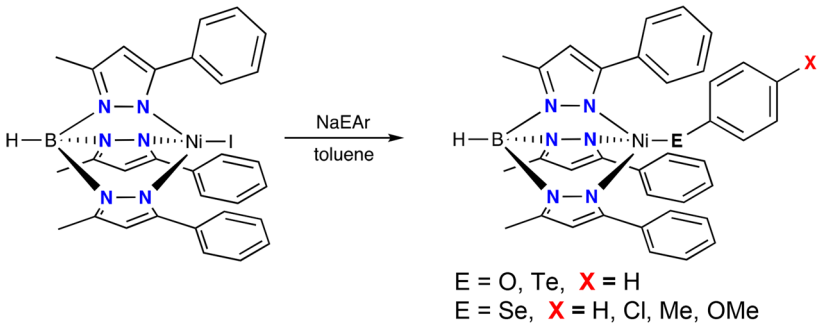

pseudo-first-order conditions in all cases. The concentrations of methyl iodide ranged from 32 to 284 mM. The reaction progress was monitored by UV−vis spectroscopy, specifically following the decrease in absorbance at λ_{max} (nm) for each [Tp^{Ph,Me}]Ni(EAr) complex. Reactions were followed to completion with rates determined by fitting 3 half-lives of data.

X-ray Structure Determination. Crystals were mounted using viscous oil onto a plastic mesh and cooled to the data collection temperature. Data were collected on a Bruker-AXS APEX II DUO CCD diffractometer with Cu Kα radiation (λ = 1.54178 Å) focused with Goebel mirrors for [Tp^{Ph,Me}]Ni(SeC$_6$H$_4$-4-OMe), and [Tp^{Ph,Me}]Ni(SeC$_6$H$_4$-4-Cl) and with graphite-monochromated Mo Kα radiation (λ = 0.71073 Å) for the other samples. Unit cell parameters were obtained from 36 data frames, 0.5° ω, from three different sections of the Ewald sphere. Samples were cooled to a collection temperature of 200 K. The data sets were treated with multiscan absorption corrections (Apex2 software suite, Madison, WI, 2005), and structures were solved using SHELXTL software.

The systematic absences in the diffraction data are uniquely consistent with $P2_1/n$ (No. 14) for [Tp^{Ph,Me}]Ni(SeC$_6$H$_5$) and [Tp^{Ph,Me}]Ni(TeC$_6$H$_5$) and with $I4_1/a$ (No. 88) for [Tp^{Ph,Me}]Ni(OC$_6$H$_5$). No symmetry higher than triclinic was observed for [Tp^{Ph,Me}]Ni(SeC$_6$H$_4$-4-Me), [Tp^{Ph,Me}]Ni(SeC$_6$H$_4$-4-OMe), and [Tp^{Ph,Me}]Ni(SeC$_6$H$_4$-4-Cl) with solutions in the centrosymmetric option, $P\bar{1}$ (No. 2), yielding chemically reasonable and computationally stable results of refinement. The data were treated with multiscan absorption corrections. The structures were solved using intrinsic phasing methods and refined with full-matrix, least-squares procedures on F^2.

Two symmetry-unique molecules were located in the asymmetric unit of [Tp^{Ph,Me}]Ni(SeC$_6$H$_5$). The initial solutions of [Tp^{Ph,Me}]Ni(OC$_6$H$_5$) and [Tp^{Ph,Me}]Ni(TeC$_6$H$_5$) showed severely disordered solvent molecules, located away from the molecules, which were treated as diffused contributions. Non-hydrogen atoms were refined with anisotropic displacement parameters. H atoms were treated as idealized contributions with geometrically calculated positions and with U_{iso} equal to 1.2U_{eq} (1.5U_{eq} for methyl) of the attached atom. Atomic scattering factors are contained in the SHELXTL program library. The structures have been deposited at the Cambridge Structural Database under the depository numbers CCDC 1893387−1893392.

Computational Details. Calculations were performed with the quantum chemical program Gaussian 09. Cartesian coordinates for the optimized structures are given in the Supporting Information. Specific calculation methods that were employed for transition-state and mechanistic analyses are as follows. First, the ground-state complexes for each of the three transition structures were fully optimized using the M06-2X exchange-correlation functional[28] with the LanL2DZ basis set.[29,30] The dissociative transition state was calculated for alkylation of the phenylselenolate anion. Vibrational frequency calculations and optimizations of the transition-state structures were performed using the same exchange functional and basis set employed for the optimizations. The resulting energies for each potential pathway are given in the Supporting Information. Additional calculations of the transition states were performed with the def2tzvpp basis set and SMD solvent model for THF. Also, another functional at the B3LYP[31] was employed and similar energetic barriers were obtained.

■ RESULTS AND DISCUSSION

Synthesis of Arylchalcogenolate Complexes. The synthesis and characterization of six new nickel(II) arylchalcogenolate complexes, [Tp^{Ph,Me}]Ni(EAr), are reported herein. The congeneric series of nickel chalcogenolate complexes consists of E = O, S,[32] Se, Te and Ar = C$_6$H$_5$. A subseries of selenolate complexes has also been synthesized to compare electronic effects arising from variation of the *para* substituent, X, on the phenylselenolate ligand (X = H, Cl, Me, OMe). A full comparison of nickel complexes throughout the chalcogen group is available by considering Jensen's previously synthesized arylthiolate nickel(II) complex [Tp^{Ph,Me}]Ni(SC$_6$H$_5$).[32]

The synthesis of each complex is accomplished through metathetical reaction of [Tp^{Ph,Me}]NiI with the sodium phenylchalcogenolate in toluene under a nitrogen atmosphere (Scheme 2). Addition of the corresponding NaEAr to a toluene solution of [Tp^{Ph,Me}]NiI resulted in an immediate color change. With the exception of the tellurium complex, each reaction mixture was stirred at room temperature for at least 12 h. Stirring the [Tp^{Ph,Me}]Ni(TeC$_6$H$_5$) solution for longer than 4 h led to decreased yields.

X-ray Crystallography of [Tp^{Ph,Me}]Ni(EAr). The molecular structures of the complete series of [Tp^{Ph,Me}]Ni phenylchalcogenolate complexes has been characterized via X-ray crystallography. A representative structure of [Tp^{Ph,Me}]Ni(SeC$_6$H$_5$) is shown in Figure 1. Their structures as a function of the chalcogen atom, as well as electronic factors of the phenylchalcogenolate ligand, have been explored. Incorporation of the different chalcogens into the Ni−EAr bond allows for a systematic structural comparison. The structural variations that arise from this chalcogen substitution are discussed herein.

The coordination geometry about the nickel center of the [Tp^{Ph,Me}]Ni(EAr) complexes is best described as pseudotetrahedral. This is indicated by the τ_4 value for four-coordinate complexes, $\tau_4 = [360 - (\alpha + \beta)]/141°$,[33] where α and β are the two largest angles, and the τ_4 value ranges from 0 (square planar) to 1 (tetrahedral). For E = O, Se, Te, τ_4 = 0. 78, 0.73, 0.73, respectively. These values correlate well with the calculated average τ_4 value for Jensen's complex [Tp^{Ph,Me}]Ni(SC$_6$H$_5$), 0.72.[34] The τ_4 values range from 0.67 to 0.78 (Table 1).

A noteworthy structural feature of these complexes is the off-axis positioning of the chalcogenolate ligand relative to the

https://doi.org/10.1021/acs.inorgchem.1c00066
Inorg. Chem. 2021, 60, 6327−6338

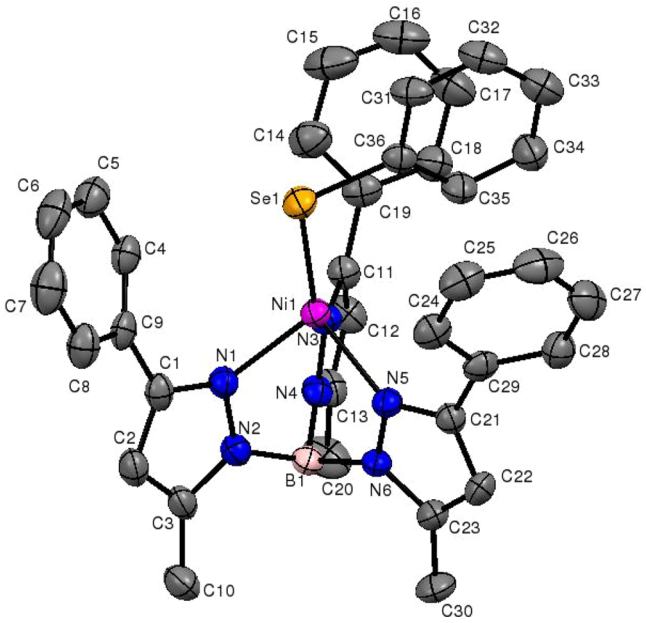

Figure 1. Thermal ellipsoid plot of [Tp^{Ph,Me}]Ni(SeC$_6$H$_5$). Thermal ellipsoids are drawn to 30% probability. Hydrogen atoms have been omitted for clarity.

pseudo-3-fold axis defined by the B- - -Ni vector. This structural phenomenon has previously been observed in several four-coordinate complexes.[34−38] The chalcogenolate ligand is tilted toward one of the pyrazoles, generating two large and one small N−Ni−E bond angle. The degree of tilt off the idealized C_3 axis varies for each chalcogenolate complex, ranging from minor distortions in the B- - -Ni−E angle, i.e. 177.69(6)° in the phenolate complex, to more significant distortions, e.g. 168.80(8)° in the tellurolate complex. These deviations from linearity stabilize the Ni−E interaction, specifically for d^8 electron configurations.[32,36,39] The off-axis position causes mixing of the filled Ni−E dσ−pσ* interaction with a singly occupied molecular orbital (SOMO). This mixing supports a more favorable E−pπ to Ni−π* interaction and a lower total energy of the molecule.[14]

Selected bond lengths for the [Tp^{Ph,Me}]Ni(EAr) complexes are given in Table 1. The Ni−E bond distances for each phenylchalcogenolate complex compare well to those of previously reported terminal chalcogenolates of nickel(II). Commencing with oxygen, there are numerous examples of structurally characterized nickel phenolate complexes. For comparison, the examples discussed herein have been limited primarily to four-coordinate tris(pyrazolyl)borate nickel complexes. The [Tp^{Ph,Me}]Ni−O bond distance of 1.813(1) Å is similar to the observed Ni−O distances in the closely related Tp^{Ph} ligand systems [Tp^{Ph}]Ni(OPh) (1.820(3) Å), [Tp^{Ph}]Ni(OPh-2,6-Me) (1.8116(14) Å), and [Tp^{Ph}]Ni(OPh-4-^{t}Bu) (1.815(2) Å).[40] Jensen has also reported two terminal phenolate complexes, one of which contains the same [Tp^{Ph,Me}]Ni fragment. Their [Tp^{Ph,Me}]Ni(O-2,6-^{i}Pr$_2$C$_6$H$_3$) complex exhibits a Ni−O distance of 1.821(1) Å, which is slightly shorter than its [Tp^{Me,Me}]Ni(O-2,6-^{i}Pr$_2$C$_6$H$_3$) counterpart at 1.841(2) Å.[41] Both distances are comparable to that of [Tp^{Ph,Me}]Ni(OC$_6$H$_5$). Two examples of structures that display comparatively longer Ni−O distances are Liaw's five-coordinate Ni(III) [Ni(OPh)(P(C$_6$H$_3$-3-SiMe$_3$-2-S)$_3$]$^-$ (1.910(3) Å)[42] and Holland's *o*-dihalophenolate [Tp^{Ph2}]Ni(2,6,dbp) (1.905(5) Å).[43] The former's longer distance is surprising given the metal's higher formal oxidation state and may be a consequence of the anionic charge. Certainly, the higher coordination number plays a role in lengthening the Ni−O bond. While the latter's longer Ni−O distance may result from steric constraints imposed by the ortho halogens on the phenoxide ring, ortho methyl groups in [Tp^{Ph}]Ni(OPh-2,6-Me) do not result in a longer Ni−O bond distance.

Structural examples of the heavier chalcogen congeners are less common. A search of the Cambridge Structural Database (CSD) for terminal nickel phenylselenolate complexes returns far fewer results. Herein for comparison are a variety of Ni−Se bond distances for complexes with diverse coordination and ligand environments. The average Ni−Se bond distance of 2.3283(8) Å in [Tp^{Ph,Me}]Ni(SeC$_6$H$_5$) is similar to those of complexes containing a terminal phenylselenolate ligand, [Ni^{II}(SePh)(P(*o*-C$_6$H$_4$S)$_2$(*o*-C$_6$H$_4$SCH$_3$)]$^-$ (2.3452(3) Å),[44] [CpNi(SePh)(PPh$_3$)] (2.303(2) Å),[45] and [(CH$_3$C(CH$_2$PPh$_2$)$_3$)Ni(SePh)] (2.301(1) Å).[46] Longer Ni−Se distances have been reported by Mascharak in the homoleptic [Ni(SePh)$_4$]$^{2-}$ (2.401(3) Å)[47] and in [Ni(DAPA)(SePh)$_2$] (DAPA = 2,6-bis[1-(phenylimino)ethyl]pyridine) (2.374(1), 2.466(1) Å).[52]

Moving further down the chalcogen group to tellurium, there have been only four reported structures of the type Ni−TeR. Among these four examples the Ni−Te distance in [Tp^{Ph,Me}]Ni(TeC$_6$H$_5$) of 2.5084(5) Å is consistent with the two complexes containing terminal phenyltellurolate ligands. These bond lengths are 2.4804(6) Å in Liaw's [CpNi(TePh)PPh$_3$]$^-$[53] and 2.486(1) Å in Kruger's [CpNi(TeC$_6$H$_3$Me$_3$)(PEt$_3$)].[54] The other example is a tellurium azamacrocycle with a larger Ni−Te bond length of 2.66 Å.[55] The final Ni−Te structure was reported by Liaw as part of a series of chalcogenolate complexes and is discussed below.[56]

While complete chalcogenolate series of nickel are rare, Liaw's *o*-amidochalcogenophenolato [Ni(−EC$_6$H$_4$-*o*-NH−)$_2$]$^-$ (E = S, Se, Te) series provides a relevant comparison. The Ni−E distances in [Tp^{Ph,Me}]Ni(EAr) are comparable to those in Liaw's series: namely, Ni−S 2.1713(6) Å, Ni−Se 2.2949(3) Å, and Ni−Te 2.4450(7) Å.[56] The increase in Ni−E bond

Table 1. Selected Bond Lengths (Å) and Angles (deg) for [Tp^{Ph,Me}]Ni(EAr) Complexes

complex	Ni−EAr (Å)	Ni−N, avg (Å)	Ni−E−Ar (Å)	τ_4
[Tp^{Ph,Me}]Ni(OC$_6$H$_5$)	1.813(1)	2.012(7)	155.3(1)	0.78
[Tp^{Ph,Me}]Ni(SC$_6$H$_5$)[32]	2.219(2)	2.011(8)	105.4(8)	0.72
[Tp^{Ph,Me}]Ni(SeC$_6$H$_5$)	2.3283(8)	2.013(3)	103.1(1)	0.73
[Tp^{Ph,Me}]Ni(SeC$_6$H$_4$-4-Cl)	2.3334(8)	2.025(3)	108.9(1)	0.68
[Tp^{Ph,Me}]Ni(SeC$_6$H$_4$-4-Me)	2.3277(4)	2.031(2)	108.90(7)	0.67
[Tp^{Ph,Me}]Ni(SeC$_6$H$_4$-4-OMe)	2.3270(4)	2.032(2)	106.95(7)	0.68
[Tp^{Ph,Me}]Ni(TeC$_6$H$_5$)	2.5084(5)	2.023(2)	103.0(1)	0.73

https://doi.org/10.1021/acs.inorgchem.1c00066
Inorg. Chem. 2021, 60, 6327−6338

Table 2. Bond Length Data (in Å) for Isostructural Terminal M−EAr Series

	$[Tp^{Ph,Me}]Ni(EAr)$	$[Tm^{But}]Cd(EAr)$[48]	$[Tm^{But}]Zn(EAr)$[49]	$Cp^*_2Zr(EAr)_2$[50]	$[Tp^{Me,Me}]_2Sm(EAr)$[51]
O	1.813(1)	2.109(6)[a]	1.925(4)	1.989(3)	2.159(2)[b]
S	2.219(2)	2.4595(7)	2.272(1)	2.522(1)	2.8620(9)[c]
Se	2.3283(8)	2.5595(5)	2.394(1)	2.651(3)	2.9390(3)
Te	2.5084(5)	2.7097(5)	2.568(1)	2.87(2)	3.1874(4)

[a]Ar = 2,6-$C_6H_3Ph_2$. [b]Ar = p-$OC_6H_4Bu^t$. [c]Ar = p-SC_6H_4Me.

distances is in agreement with observed trends in chalcogen atomic radii. Analogous trends in bond lengths are visible in similar isostructural arylchalcogenolate series[48−51] (Table 2).

Among the $[Tp^{Ph,Me}]Ni$ arylchalcogenolate complexes, modification of the chalcogen has little effect on the Ni−N bond lengths. The Ni−E−Ar bond angles decrease on descending the chalcogen group: O > S > Se > Te. The most significant decrease is observed on moving from O (155.3°) to S (105.4°). The difference between oxygen and sulfur is 49.9°, whereas in a move to heavier chalcogens among the arylchalcogenolates, the difference in bond angles varies by 2°. This decrease in Ni−E−Ar bond angles follows the trend for the experimentally determined angles of H_2E molecules: H_2O (104.5°), H_2S (92.2°), H_2Se (91.0°), and H_2Te (89.5°).[57] Here, it is also evident that the largest difference in bond angles throughout the chalcogen series occurs between oxygen and sulfur. For the H_2E series, the angle is driven by electronics, whereas in the Ni series, the substituent steric effects are more pronounced. The wider angle in both $[Tp^{Ph,Me}]Ni(OC_6H_5)$ and H_2O are ascribed to hybridized bonding, whereas in the heavier chalcogens p-type σ-bonds are the norm.[50,58]

A series of $[Tp^{Ph,Me}]Ni(SeAr)$ analogues with electronic modifications at the *para* position of the arylselenolate ligand have been characterized structurally. These nickel(II) phenylselenolate complexes include $[Tp^{Ph,Me}]Ni(SeC_6H_4\text{-}4\text{-}X)$ (X = H, Cl, Me, OMe). While the structural effects of chalcogen variation were discernible, structural influences from the *para* substituents were not as apparent among the arylselenolate series. There is a very modest correlation between Ni−SeAr bond length and the electron-donating ability of the selenolate ligand. The more electron donating substituents, *p*-OMe and *p*-Me, exhibit shorter Ni−SeAr bond distances, whereas the electron-withdrawing *p*-Cl substituent leads to a slightly elongated Ni−SeAr bond distance (Table 1). Introduction of the *para* substituent leads to enhanced tilting off of the ideal C_3 axis (τ_4(avg) = 0.68), as well as an increase in the Ni−SeAr bond angles. The differences in bond angles are modest with no discernible trend. The minor variations are most likely influenced by steric and/or crystal-packing effects rather than electronic effects.

^{1}H NMR Spectroscopy. The series of nickel(II) arylchalcogenolate complexes consists of a high-spin, S = 1, nickel center. Therefore, these complexes have been investigated using paramagnetic ^{1}H NMR spectroscopy, wherein the complexes exhibit broad signals over a wide chemical shift range. The spectra are well-resolved in C_6D_6 solution at room temperature with characteristic resonances assigned to the $[Tp^{Ph,Me}]Ni(EAr)$ complexes (Figure 2).

The protons on the Tp ligand backbone, as well as on the arylchalcogenolate substituent, provide excellent markers for tracking the effect of chalcogen on the chemical shifts. The pattern observed for these arylchalcogenolate resonances is an alternating upfield, downfield, upfield shift for *ortho*, *meta*, and

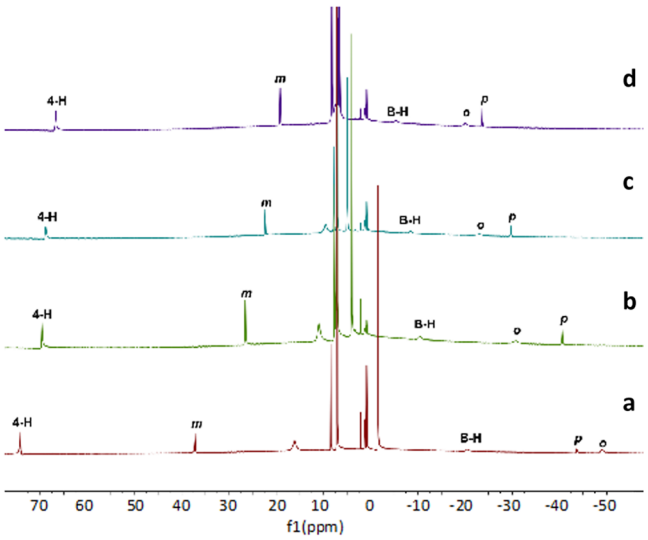

Figure 2. ^{1}H NMR spectra of $[Tp^{Ph,Me}]Ni(EAr)$ in C_6D_6 recorded at room temperature: (a) E = O, red; (b) E = S, green; (c) E = Se, teal; (d) E = Te, purple.

para signals, respectively. These hyperfine-shifted signals are indicative of a spin polarization pathway, which results from the unpaired spins on the paramagnetic nickel center. The spins on the neighboring atoms are polarized in an alternating parallel and antiparallel manner, such that the corresponding ^{1}H NMR signals occur downfield for parallel spins and upfield for antiparallel spins.[59,60] This presentation of chemical shifts is well documented in other paramagnetic metal complexes.[32,34,61,62]

Further comparison of the ^{1}H NMR spectra for the different chalcogen-substituted complexes reveals a gradual shift of the paramagnetic signals toward the diamagnetic region. This effect correlates to the effective magnetic moments of the arylchalcogenolate complexes, which were determined in solution by the Evans method.[27] The larger magnetic moments are associated with greater paramagnetic shifts (Table 3). A similar trend was observed in Midollini's $(Et_4N)_3[Fe_4E_4(SPh)_4]$ (E = S, Se, Te) complexes. In these iron ferredoxin models, it was observed that larger magnetic moments correlated to greater paramagentic shifts in the ^{1}H NMR spectra. Interestingly, Fe_4Te_4 exhibited the largest magnetic moment.[63]

Table 3. Magnetic Data and ^{1}H NMR Chemical Shifts at 298 K for $[Tp^{Ph,Me}]Ni(EAr)$ Complexes

	μ_{eff} (μ_B)	δ(ppm): *o*-H, *m*-H, *p*-H
$[Tp^{Ph,Me}]Ni(OC_6H_5)$	3.04(4)	−48.9, 37.2, −43.6
$[Tp^{Ph,Me}]Ni(SC_6H_5)$	2.88(4)	−30.7, 26.5, −40.7
$[Tp^{Ph,Me}]Ni(SeC_6H_5)$	2.80(4)	−23.0, 22.3, −29.8
$[Tp^{Ph,Me}]Ni(TeC_6H_5)$	2.73(1)	−20.2, 19.2, −23.7

https://doi.org/10.1021/acs.inorgchem.1c00066
Inorg. Chem. 2021, 60, 6327−6338

The *para*-substituted selenolate series $[Tp^{Ph,Me}]Ni(SeC_6H_4$-4-X) shows similar trends in their ^1H NMR spectra (Figure 3).

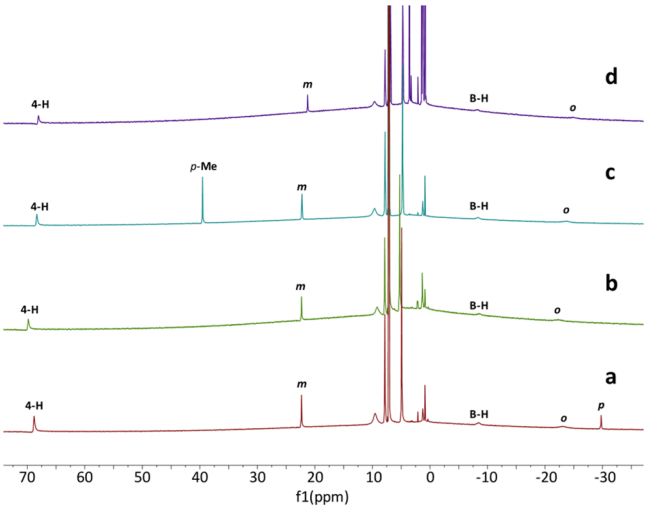

Figure 3. ^1H NMR spectra of $[Tp^{Ph,Me}]Ni(SeC_6H_4$-X) in C_6D_6 recorded at room temperature: (a) X = H, red; (b) X = Cl, green; (c) X = Me, teal; (d) X = OMe, purple.

However, there are only minor differences in chemical shifts as the *para* substituent is varied from X = Cl, H, Me to OMe. While the chemical shifts vary to a small degree among the arylselenolate derivatives, a general trend is apparent. An increase in the electron-donating ability of the aryl selenolate ligand from Cl to OMe is related to a very small decrease in the downfield pyrazole 4-H proton shift from 69.8 to 68.1 ppm. This occurs with a concomitant upfield shift of the arylselenolate *ortho* protons from −22.2 to −24.9 ppm. In addition, upon replacement of the *para* substituent with a methyl group the ^1H NMR spectrum exhibits further evidence of spin polarization. On replacement of the *p*-H shifted upfield, the protons of the *p*-methyl group appear downfield due to the alternating parallel and antiparallel spins.

Electronic Spectroscopy. The electronic absorption spectra of $[Tp^{Ph,Me}]Ni(EAr)$ display intense absorption features in the visible region corresponding to ligand to metal charge transfer (LMCT) bands (Figure 4). These transitions are assigned to an E−Ni pπ−dπ* charge transfer.[11,32,58,62] The bands range in energy from 430 to 670 nm, with the highest energy band assigned to E = OPh and the lowest energy band assigned to E = TePh. The observed red shift in energies on moving down the series is reflective of the comparative electronegativities of the chalcogens. On descending the chalcogen series, there is a decrease in the electronegativity. In the chalcogenolate complexes this is associated with an increase in the energy of the ligand pπ orbital, resulting in a smaller transition energy between ligand pπ and metal dπ* orbitals.

Figure 4 displays the analogous LMCT bands for the $[Tp^{Ph,Me}]Ni(SeC_6H_4$-4-X) complexes. In order of increasing electron-donating ability of the chalcogenolate ligand, Cl to OMe, a minor red shift from 570 to 600 nm is noted. The red shift in this *para*-substituted selenolate series can be rationalized in the same manner as for the arylchalcogenolates. Specifically, the change in energy of the ligand pπ orbital is associated with the change in the magnitude of the LMCT band energy. Jensen and co-workers have characterized a

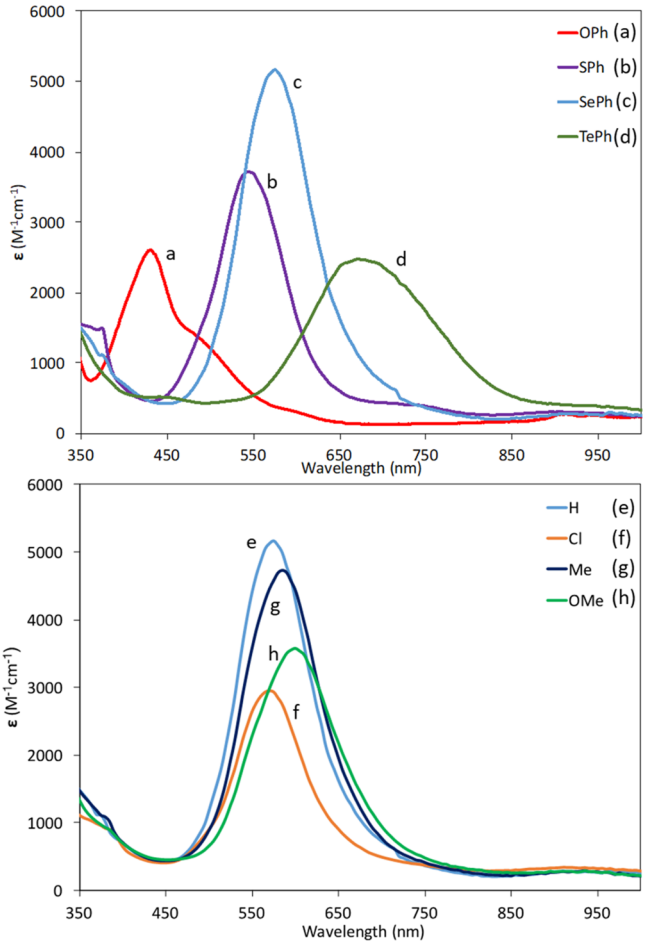

Figure 4. Electronic absorption spectra of $[Tp^{Ph,Me}]Ni(EAr)$ (top) and $[Tp^{Ph,Me}]Ni(SeC_6H_4$-4-X) (bottom), recorded in THF at room temperature.

related nickel(II) thiolate series with $Tp^{Ph,Me}$ and $Tp^{Me,Me}$ ligands.[34,39] Their $[Tp^{R,Me}]Ni(SC_6H_4$-4-X) series (R = Me, Ph; X = H, Cl, Me, OMe) shows similar absorption bands in the visible region: 506 nm for R = Me and 540 nm for R = Ph.

Electrophilic Alkylation Reactivity. All reactions of $[Tp^{Ph,Me}]Ni(EAr)$ were performed in dry THF at room temperature under pseudo-first-order conditions: i.e., [MeI] > 100[$[Tp^{Ph,Me}]Ni(EAr)$]. Solutions of the intensely colored arylchalcogenolate complexes turn pale orange over the course of the reaction. $[Tp^{Ph,Me}]NiI$ formation was confirmed by electronic absorption (λ_{max} = 390, 435 nm in THF) and ^1H NMR spectroscopies (δ 75.1 ppm in C_6D_6). The identity of the organic product was confirmed by gas chromatography−mass spectrometry (GC-MS) and ^1H NMR spectroscopy.

The reactions of $[Tp^{Ph,Me}]Ni(EAr)$ with MeI occur readily at room temperature on a time scale ideal for kinetic analysis. Depending on the identity of the chalcogen, the alkylation reaction time courses vary on the order of minutes to several hours. Consequently, electronic absorption spectroscopy provides a practical method for measuring the reaction rates. The loss of the LMCT absorption bands gave rise to the absorption features of the product, $[Tp^{Ph,Me}]NiI$, with observation of an isosbestic point, indicative of an optically clean reaction (Figure 5).

The time-dependent decrease in concentration of the starting material at λ_{max} exhibited exponential decay over the

https://doi.org/10.1021/acs.inorgchem.1c00066
Inorg. Chem. 2021, 60, 6327−6338

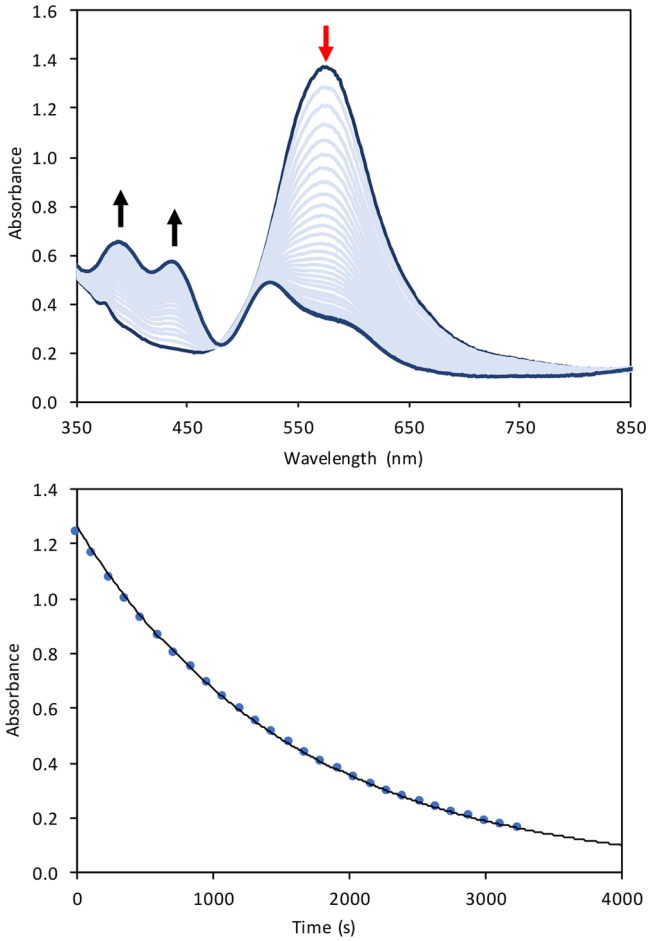

Figure 5. (top) Electronic absorption spectra monitoring the decrease in λ_{max} at 580 nm for the reaction of $[Tp^{Ph,Me}]Ni(SeC_6H_5)$ with methyl iodide (284 mM) in THF at 25 °C. (bottom) Exponential decay time course of the same reaction.

course of 3 half-lives. A representative plot for one of these reactions is depicted in Figure 5. A pseudo-first-order plot was constructed to derive k_{obs} from the linear relationship of $\ln[(A - A_\infty)/(A_i - A_\infty)]$ versus time. The k_{obs} values for each reaction were measured over a range of MeI concentrations. The reactions demonstrated second-order kinetics, first order in each reagent. Second-order rate constants, k_2, for each reaction were obtained from the linear relationship of k_{obs} versus [MeI] (Figure 6).

$[Tp^{Ph,Me}]Ni(OC_6H_5)$ did not react with methyl iodide even under more forcing reaction conditions of 70 °C for several days. Notably, the small positive intercept for the alkylation of $[Tp^{Ph,Me}]Ni(TeC_6H_5)$ suggests a side reaction, which is ascribed to competitive decomposition of the complex due to its instability in solution.

The trend in the observed reaction rate is O (no reaction) ≪ S < Se < Te (Table 4). While the data contained therein are for reactions conducted in THF, additional reactions were performed in toluene. Reactions in the less polar toluene exhibited a significantly slower rate in comparison to those in THF. Incidentally, it is relevant that Jensen has determined the k_2 value for alkylation of the complex $[Tp^{Ph,Me}]Ni(SC_6H_5)$ with MeI in 1,2-dichloroethane.[64] The k_2 value for this reaction is $1.83(4) \times 10^{-3}$ M^{-1} s^{-1}. This value is larger than that for the same complex's rate constant measured in THF (Table 4). Similarly to the reactions conducted in toluene, this result

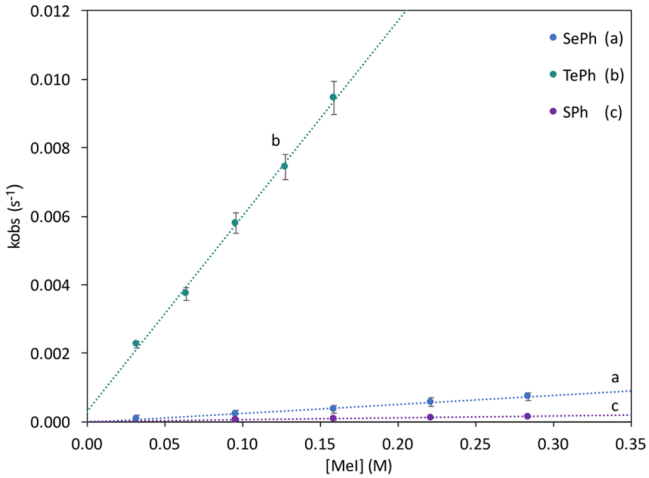

Figure 6. Plot of k_{obs} vs [MeI] for each $[Tp^{Ph,Me}]Ni(EAr)$ complex used in determining k_2 for the reaction with methyl iodide. Error bars are included for each data set; where error bars are not visible, they are within the size of the data point.

Table 4. Second-Order Rate Constants for Alkylation Reactions with MeI in THF

complex	k_2, M^{-1} s^{-1}
$[Tp^{Ph,Me}]Ni(SC_6H_5)$	$3.9(3) \times 10^{-4}$
$[Tp^{Ph,Me}]Ni(SeC_6H_5)$	$2.6(3) \times 10^{-3}$
$[Tp^{Ph,Me}]Ni(SeC_6H_4\text{-}4\text{-}Cl)$	$9.8(2) \times 10^{-4}$
$[Tp^{Ph,Me}]Ni(SeC_6H_4\text{-}4\text{-}Me)$	$3.6(1) \times 10^{-3}$
$[Tp^{Ph,Me}]Ni(SeC_6H_4\text{-}4\text{-}OMe)$	$4.7(5) \times 10^{-3}$
$[Tp^{Ph,Me}]Ni(TeC_6H_5)$	$5.7(5) \times 10^{-2}$

provides further evidence that more polar solvents accelerate the rate of the reaction. The solvent effect on reaction rate is consistent with the alkylation reactions proceeding via an S_N2 mechanism. In sum, the observed trend in reactivity among the chalcogenolates parallels an increase in nucleophilicity among the heavier chalcogens.

The complete examination of reactivity of the chalcogen series from oxygen to tellurium presented herein represents the first such reactivity study of which we are aware. Therefore, relevant systematic comparisons are not possible. However, further insight is gained by assessing the rates of reactivity between the more prevalent sulfur and selenium nucleophiles. Reactions of organic thiolates and selenolates with methyl iodide are well-known. Songstad determined several nucleophilic reactivity constants with methyl iodide, including a variety of sulfur and selenium substrates.[65,66] For reactions of PhENa and $(Me)_2E$ where E = S, Se, the ratio k_{Se}/k_S ranges from 5.9 to 6.5, indicating faster reactions for both anionic and neutral selenium species. By comparison $k_{Se}/k_S = 6.7$ for the $[Tp^{Ph,Me}]Ni(EPh)$ complexes. In the current series, on transitioning to the heavier tellurolate congener, the reaction with MeI is ∼22 times faster than that with the selenolate and ∼146 times faster than that with the thiolate.

Eyring Analysis. An Eyring analysis was conducted for the reaction of $[Tp^{Ph,Me}]Ni(SeC_6H_5)$ with MeI to deduce activation parameters. Reactions with concentrations of MeI at 284 mM were performed over a 40 °C temperature range, 15−55 °C. Plotting $\ln(k/T)$ versus $1/T$ for five distinct temperatures yielded a linear relationship (Figure 7). The activation parameters for this second-order reaction were determined to be $\Delta H^\ddagger = 12(1)$ kcal mol^{-1} and $\Delta S^\ddagger = -33(3)$

https://doi.org/10.1021/acs.inorgchem.1c00066
Inorg. Chem. 2021, 60, 6327−6338

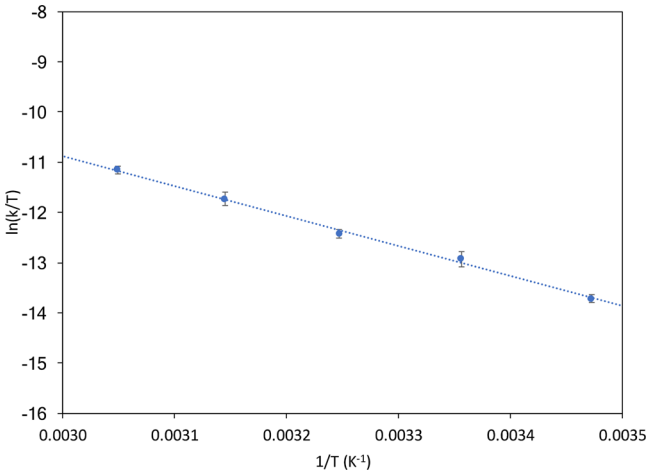

Figure 7. Eyring plot of k_2 (M^{-1} s^{-1}) for the reaction of $[Tp^{Ph,Me}]Ni(SeC_6H_5)$ with MeI in THF.

cal mol^{-1} K^{-1}. Alkylation reactions for complexes with terminal thiolate ligands have been reported to have similar values. Notably, the activation parameters for reaction of Jensen's $[Tp^{Ph,Me}]Ni(SMes)$ with MeI are the same within error: $\Delta H^{\ddagger}$ = 11(1) kcal mol^{-1} and $\Delta S^{\ddagger}$ = −37(4) cal mol^{-1} K^{-1}.[64] At first glance, it would appear that these activation parameters are consistent with an associative substitution mechanism. Indeed, the small enthalpic value is consistent with an S_N2 transition state. Likewise, the negative entropic term is indicative of an ordered transition state in an associative mechanism. However, these parameters alone are insufficient in distinguishing between associative and dissociative pathways. For instance, a negative entropy value could be the result of solvent electrostriction, due to solvated anions and cations in a dissociative reaction, for example, as detailed by Parkin.[23]

In Jensen's electrophilic alkylation of nickel(II) arylthiolates, evidence for a possible associative mechanism was cited, but they did not discount a dissociative mechanism. Alkylation in separate systems can have similar activation parameters and operate under different mechanisms. Our laboratory[22] and that of Parkin[23] reported similar values for alkylation of Zn thiolates with MeI: $\Delta H^{\ddagger}$ = 16 kcal mol^{-1}, $\Delta S^{\ddagger}$ = −20 cal mol^{-1} K^{-1} and $\Delta H^{\ddagger}$ = 14.1(1) kcal mol^{-1}, $\Delta S^{\ddagger}$ = −23.1(4) cal mol^{-1} K^{-1}, respectively. Despite deriving comparable activation parameters, the reactivity of our laboratory's $[Ph(pz^tBu)Bt^tBu]Zn(SAr)$ complex with MeI was proposed to occur via an associative route, whereas Parkin's $[Tm^{Ph}]Zn(SCH_2C(O)N(H)Ph)$ was proposed to proceed via a dissociative mechanism.

Electron-Donating Effects/Hammett Relationship. The alkylation kinetics of $[Tp^{Ph,Me}]Ni(EAr)$ complexes were explored via the series of *para*-substituted phenylselenolate complexes, $[Tp^{Ph,Me}]Ni(SeC_6H_4\text{-}4\text{-}X)$ (X = Cl, Me, OMe). The reactions were performed with MeI under the same conditions as those for the arylchalcogenolate analogues. The results are presented in Table 4 and Figure 8. Analogously to the phenylchalcogenolate derivatives, the phenylselenolate complexes exhibited a linear relationship for k_{obs} and [MeI], consistent with a first-order dependence on the alkyl halide. Reaction rates increase in the order Cl < H < Me < OMe. The more strongly electron donating substituents on the phenylselenolate ligand contribute to faster reaction rates.

In analyzing the effect of electron-donating and -withdrawing substituents on the rate of the reaction, a Hammett

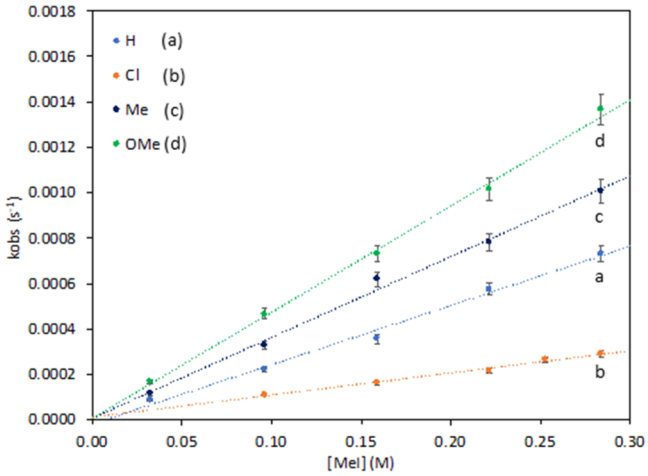

Figure 8. Plot of k_{obs} vs [MeI] for each $[Tp^{Ph,Me}]Ni(SeC_6H_4\text{-}4\text{-}X)$ complex used in determining k_2 for the reaction with methyl iodide. Error bars are included for each data set; where error bars are not visible, they are within the size of the data point.

plot was constructed (Figure 9). By a plot of k_2 values for the arylselenolate derivatives against the standard Hammett

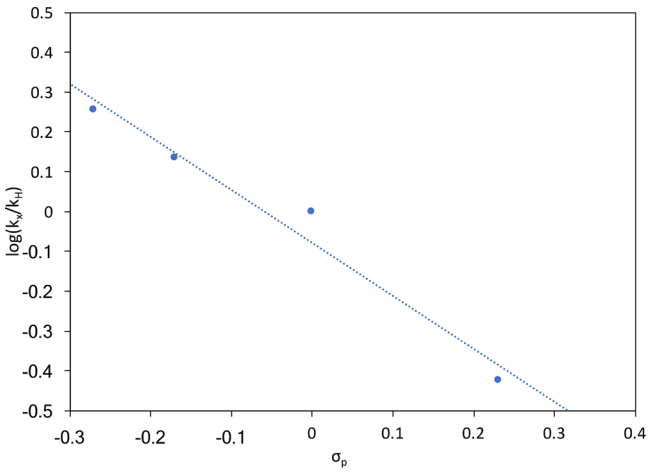

Figure 9. Hammett plot for the reactions of $[Tp^{Ph,Me}]Ni(SeC_6H_4\text{-}4\text{-}X)$ with MeI in THF at 25 °C. From left to right the data points represent X = OMe, Me, H, Cl.

substituent constants (σ_p),[67] the Hammett reaction constant (ρ) was determined. The ρ value is used to gain insight into the reaction mechanism. For alkylations of $[Tp^{Ph,Me}]Ni(SeC_6H_4\text{-}4\text{-}X)$ with MeI, ρ = −1.3(3). A negative ρ value is indicative of accumulation of charge in the transition state, specifically a buildup of positive charge.[68] On consideration of the two mechanisms discussed earlier (Scheme 1), in an associative transition state, this could indicate stabilization of positive charge accumulation on selenium by the more electron donating substituents. However, there is also charge accumulated in a dissociative transition state. In this case, ρ would depend on the ability of the phenylselenolate ligand to dissociate, as well as the strength of the dissociated nucleophile.[64] Similar ρ values have been reported for nickel complexes with terminal thiolate ligands. For reactions with benzyl bromide in toluene, Guan obtained ρ = −1.5(3) for a square-planar nickel(II) complex[69] and Jensen's $[Tp^{Ph,Me}]Ni$ arylthiolate complexes yielded ρ = −1.7(4).[64] While the

https://doi.org/10.1021/acs.inorgchem.1c00066
Inorg. Chem. 2021, 60, 6327−6338

Hammett reaction constants compare favorably, the reaction mechanisms for each of these systems remain to be elucidated. Therefore, to gain further insight into the details of the mechanism, DFT computational methods were employed to buttress the experimental results.

Computational Analysis. To obtain greater insight into the mechanistic pathway of the electrophilic alkylation reactions of $[Tp^{Ph,Me}]Ni(EAr)$ with MeI, DFT computational methods were employed. In accordance with the experimentally determined activation parameters for the reaction of $[Tp^{Ph,Me}]Ni(SeC_6H_5)$ with MeI, this reaction was used as the model system for computational analysis. The transition states for each of three pathways were modeled, Scheme 1. Two transition states were considered for the individual associative mechanisms, i.e. classical S_N2 and four-centered, and one transition state for the potential dissociative route. The resulting energies for the potential pathways are contained in Tables S1 and S2 in the Supporting Information.

From the transition-state calculations, it is evident that the reaction barriers for a four-centered associative transition state and dissociation of the arylselenolate are quite high for a reaction that occurs readily at room temperature. Energetic values for the classical S_N2 transition structure showed greater potential for a mechanism that proceeds through this transition state, but the computed enthalpy of reaction, $\Delta H^{\ddagger}$ = 23.6 kcal mol^{-1}, was much greater than the experimentally determined value, $\Delta H^{\ddagger}$ = 12(1) kcal mol^{-1}. Further consideration was given to the solvated model for the S_N2 associative transition state. Using the SMD solvent model in THF, the theoretically determined enthalpy, $\Delta H^{\ddagger}$ = 17.3 kcal mol^{-1}, showed somewhat better agreement with the experimentally derived value for the reaction with MeI. Upon selection of a larger basis set, Def2TZVPP, the enthalpy was lowered even further to $\Delta H^{\ddagger}$ = 14.1 kcal mol^{-1}. This calculated value compares well with the experimentally determined value, $\Delta H^{\ddagger}$ = 12(1) kcal mol^{-1}. On the basis of these calculations, the electrophilic alkylation of $[Tp^{Ph,Me}]Ni(EAr)$ with MeI is proposed to proceed via an associative mechanism, through a classical S_N2 transition state (Figure 10).

Although several studies have been conducted to elucidate the electrophilic alkylation mechanism of metal−thiolates,[21,22,64,70] less commonly have computational methods been deployed as a means to complement and buttress mechanistic arguments.[71] One study that did include DFT calculations in their analysis of the alkylation mechanism was Parkin's examination of Zn thiolates.[23] Experimentally, it was determined that the reaction of $[Tm^{Ph}]ZnSCH_2C(O)NHPh$ with MeI had a small kinetic isotope effect (KIE) of k_H/k_D = 1.16(1) at 0 °C. When both associative and dissociative transition states were modeled, calculations were supportive of a dissociative mechanism due to a determined KIE value of 1.08 at 0 °C, which compared well with experimental results. In Parkin's study of Zn−thiolates and the work presented herein on nickel chalcogenolates, a computational analysis of transition states proved to be an effective tool for distinguishing between associative and dissociative routes. From these results, it is clear that mechanistic analyses of alkylation reactions can benefit from supplemental computational analysis.

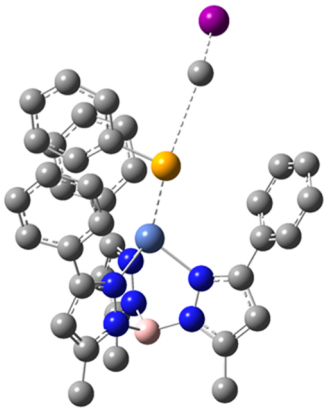

Figure 10. Geometry-optimized structure of the $[Tp^{Ph,Me}]Ni(SeC_6H_5)$- - -Me- - -I transition state. Hydrogens have been omitted for clarity.

■ SUMMARY

The synthesis and characterization of the complete congeneric $[Tp^{Ph,Me}]Ni(EAr)$ series has allowed for a systematic comparison of nickel chemistry throughout the chalcogen group. Structural changes arising from variation of the chalcogen were consistent with periodic trends. Ni−E bond lengths increase from E = O to Te, whereas Ni−E−Ar bond angles decrease, corresponding to changes in the chalcogen. Additionally, electronic effects were considered through characterization of the phenylselenolate *para*-substituted series, $[Tp^{Ph,Me}]Ni(SeC_6H_4\text{-}4\text{-}X)$ (X = Cl, Me, OMe). There were only minor changes in Ni−E bond length, with shorter bond distances correlating to more electron donating substituents. Overall, substitution of the different chalcogens had a greater effect on the structural parameters in comparison to electronic substitution on the arylchalcogenolate ligand.

The ^{1}H NMR spectra of $[Tp^{Ph,Me}]Ni(EAr)$ complexes displayed paramagnetic contact shifts, with evidence of a spin-polarization pathway. The spectra also indicated a correlation between μ_{eff} and the degree of shifting toward the paramagnetic region. Furthermore, the electronic absorption spectra showed intense LMCT features in the visible region, which displayed a red shift in energies corresponding to either a decrease in electronegativity of the chalcogen or an increase in the electron-donating ability of the ligand.

A detailed kinetic analysis of electrophilic alkylation reactions of $[Tp^{Ph,Me}]Ni(EAr)$ with methyl iodide provided insight into reaction trends among the chalcogens, as well as a greater mechanistic understanding. Reactions conducted at room temperature in THF exhibited second-order kinetics, first order in each reactant. Rates increased from E = O to Te corresponding to an increase in chalcogen nucleophilicity. An analysis of reaction rates under the same conditions for $[Tp^{Ph,Me}]Ni(SeC_6H_4\text{-}4\text{-}X)$ showed faster rates coincident with greater electron-donating ability of the arylselenolate ligand: X = OMe > Me > H > Cl. Furthermore, activation parameters for the alkylation reaction were considered for $[Tp^{Ph,Me}]Ni(SeC_6H_5)$ resulting in the values $\Delta H^{\ddagger}$ = 12(1) kcal mol^{-1} and $\Delta S^{\ddagger}$ = −33(3) cal mol^{-1} K^{-1}. An associative mechanism, proceeding through a S_N2 transition state, was proposed on the basis of DFT transition-state calculations. Other factors were considered in distinguishing between associative and dissociative mechanisms, such as exchange reactions, electronic effects, and the Hammett reaction constant. DFT analysis provided the most convincing evidence in support of an associative mechanism.

https://doi.org/10.1021/acs.inorgchem.1c00066
Inorg. Chem. 2021, 60, 6327−6338

■ ASSOCIATED CONTENT

Supporting Information

The Supporting Information is available free of charge at https://pubs.acs.org/doi/10.1021/acs.inorgchem.1c00066.

Thermal ellipsoid plots of X-ray structures, calculated reaction barrier energies, and Cartesian coordinates of optimized DFT structures (PDF)

Accession Codes

CCDC 1893387−1893392 contain the supplementary crystallographic data for this paper. These data can be obtained free of charge via www.ccdc.cam.ac.uk/data_request/cif, or by emailing data_request@ccdc.cam.ac.uk, or by contacting The Cambridge Crystallographic Data Centre, 12 Union Road, Cambridge CB2 1EZ, UK; fax: +44 1223 336033.

■ AUTHOR INFORMATION

Corresponding Author

Charles G. Riordan − *Department of Chemistry and Biochemistry, University of Delaware, Newark, Delaware 19716, United States*; orcid.org/0000-0002-8572-4571; Email: riordan@udel.edu

Authors

Lauren L. Cordeiro − *Department of Chemistry and Biochemistry, University of Delaware, Newark, Delaware 19716, United States*

Olga Dmitrenko − *Department of Chemistry and Biochemistry, University of Delaware, Newark, Delaware 19716, United States*

Glenn P. A. Yap − *Department of Chemistry and Biochemistry, University of Delaware, Newark, Delaware 19716, United States*

Complete contact information is available at: https://pubs.acs.org/10.1021/acs.inorgchem.1c00066

Notes

The authors declare no competing financial interest.

Adapted from Cordiero, L. M. Synthesis and Reactivity Studies of Nickel Arylchalcogenolate Complexes. Ph.D. Thesis, University of Delaware, Newark, DE, 2018, http://udspace.udel.edu/handle/19716/23960.

■ ACKNOWLEDGMENTS

Support from the University of Delaware's Department of Chemistry & Biochemistry is greatly appreciated.

■ REFERENCES

(1) Mason, A.; Coates, G. W. New Phenoxyketimine Titanium Complexes: Combining Isotacticity and Living Behavior in Propylene Polymerization. *J. Am. Chem. Soc.* **2004**, *126*, 16326−16327.

(2) Agapie, T.; Day, M. W.; Bercaw, J. E. Synthesis and Reactivity of Tantalum Complexes Supported by Bidentate X2 and Tridentate LX_2 Ligands with Two Phenolates Linked to Pyridine, Thiophene, Furan, and Benzene Connectors: Mechanistic Studies of the Formation of a Tantalum Benzylidene and Insertion Chemistry for Tantalum−Carbon Bonds. *Organometallics* **2008**, *27*, 6123−6142.

(3) Sampson, J.; Choi, G.; Akhtar, M. N.; Jaseer, E. A.; Therayalappil, R.; Al-Muallem, H. A.; Agapie, T. Olefin Polymerization by Dinuclear Zirconium Catalysts Based on Rigid Teraryl Frameworks: Effects on Tacticity and Copolymerization Behavior. *Organometallics* **2017**, *36*, 1915−1928.

(4) Egorova, M.; Prins, R. Hydrodesulfurization of dibenzothiophene and 4,6-dimethyldibenzothiophene over sulfided NiMo/γ-Al2O3, CoMo/γ-Al_2O_3, and Mo/γ-Al_2O_3 catalysts. *J. Catal.* **2004**, *225*, 417−427.

(5) Deo, S. R.; Singh, A. K.; Deshmukh, L.; Susan, M. A. Metal Chalcogenide Nanocrystalline Solid Thin Films. *J. Electron. Mater.* **2015**, *44*, 4098−4127.

(6) Huang, R. W.; Wei, Y. S.; Dong, X. Y.; Wu, X. H.; Du, C. X.; Zang, S. Q.; Mak, T. C. W. Hypersensitive dual-function luminescence switching of a silver-chalcogenolate cluster-based metal−organic framework. *Nat. Chem.* **2017**, *9*, 689−697.

(7) Lee, Y. W.; Kim, B. S.; Hong, J.; Choi, H.; Jang, H. S.; Hou, B.; Pak, S.; Lee, J.; Lee, S. H.; Morris, S. M.; Whang, D.; Hong, J. P.; Shin, H. S.; Cha, S.; Sohn, J. I.; Kim, J. M. Hierarchically assembled tubular shell-core-shell heterostructure of hybrid transition metal chalcogenides for high-performance supercapacitors with ultrahigh cyclability. *Nano Energy* **2017**, *37*, 15−23.

(8) Jiang, P.; Zhu, D. L.; Zhu, C. N.; Zhang, Z. L.; Zhang, G. J.; Pang, D. W. A highly reactive chalcogenide precursor for the synthesis of metal chalcogenide quantum dots. *Nanoscale* **2015**, *7*, 19310−19316.

(9) Li, X.; Shan, J. Y.; Zhang, W. Z.; Su, S.; Yuwen, L. H.; Wang, L. H. Recent Advances in Synthesis and Biomedical Applications of Two-Dimensional Transition Metal Dichalcogenide Nanosheets. *Small* **2017**, *13*, 1602660.

(10) Holm, R. H.; Kennepohl, P.; Solomon, E. I. Structural and Functional Aspects of Metal Sites in Biology. *Chem. Rev.* **1996**, *96*, 2239−2314.

(11) Solomon, E. I.; Gorelsky, S. I.; Dey, A. Metal−thiolate bonds in bioinorganic chemistry. *J. Comput. Chem.* **2006**, *27*, 1415−1428.

(12) Solomon, E. I.; Szilagyi, R. K.; George, S. D.; Basumallick, L. Electronic Structures of Metal Sites in Proteins and Models: Contributions to Function in Blue Copper Proteins. *Chem. Rev.* **2004**, *104*, 419−458.

(13) Meunier, B.; de Visser, S. P.; Shaik, S. Mechanism of Oxidation Reactions Catalyzed by Cytochrome P450 Enzymes. *Chem. Rev.* **2004**, *104*, 3947−3980.

(14) Sheng, Y. W.; Abreu, I. A.; Cabelli, D. E.; Maroney, M. J.; Miller, A. F.; Teixeira, M.; Valentine, J. S. Superoxide dismutases and superoxide reductases. *Chem. Rev.* **2014**, *114*, 3854−3918.

(15) Bouwman, E.; Reedijk, J. Structural and functional models related to the nickel hydrogenases. *Coord. Chem. Rev.* **2005**, *249*, 1555−1581.

(16) Ragsdale, S. W. Metals and Their Scaffolds To Promote Difficult Enzymatic Reactions. *Chem. Rev.* **2006**, *106*, 3317−3337.

(17) (a) Riordan, C. G. Acetyl coenzyme A synthase: new insights into one of Nature's bioorganometallic catalysts. *J. Biol. Inorg. Chem.* **2004**, *9*, 509−510. (b) Riordan, C. G. Synthetic Chemistry and Chemical Precedents for Understanding the Structure and Function of Acetyl Coenzyme A Synthase. *J. Biol. Inorg. Chem.* **2004**, *9*, 542−549.

(18) Parkin, G. Synthetic analogues relevant to the structure and function of zinc enzymes. *Chem. Rev.* **2004**, *104*, 699−767.

(19) Myers, L. C.; Terranova, M. P.; Ferentz, A. E.; Wagner, G.; Verdine, G. L. Repair of DNA methylphosphotriesters through a metalloactivated cysteine nucleophile. *Science* **1993**, *261*, 1164−1167.

(20) Lin, Y. X.; Dotsch, V.; Wintner, T.; Peariso, K.; Myers, L. C.; Penner-Hahn, J. E.; Verdine, G. L.; Wagner, G. Structural Basis for the Functional Switch of the E. coli Ada Protein. *Biochemistry* **2001**, *40*, 4261−4271.

(21) Wilker, J. J.; Lippard, S. J. Alkyl Transfer to Metal Thiolates: Kinetics, Active Species Identification, and Relevance to the DNA Methyl Phosphotriester Repair Center of Escherichia coli Ada. *Inorg. Chem.* **1997**, *36*, 969−978.

(22) Chiou, S. J.; Riordan, C. G.; Rheingold, A. L. Synthetic modeling of zinc thiolates: Quantitative assessment of hydrogen bonding in modulating sulfur alkylation rates. *Proc. Natl. Acad. Sci. U. S. A.* **2003**, *100*, 3695−3700.

(23) Morlok, M. M.; Janak, K. E.; Zhu, G.; Quarless, D. A.; Parkin, G. Intramolecular NH···S Hydrogen Bonding in the Zinc Thiolate Complex $[Tm^{Ph}]ZnSCH_2C(O)NHPh$: A Mechanistic Investigation

of Thiolate Alkylation as Probed by Kinetics Studies and by Kinetic Isotope Effects. *J. Am. Chem. Soc.* **2005**, *127*, 14039−14050.
(24) Brand, U.; Rombach, M.; Seebacher, J.; Vahrenkamp, H. Functional Modeling of Cobalamine-Independent Methionine Synthase with Pyrazolylborate−Zinc−Thiolate Complexes. *Inorg. Chem.* **2001**, *40*, 6151−6157.
(25) Clemenceau, A.; Wang, Q.; Zhu, J. P. Enantioselective Synthesis of Quaternary α-Amino Acids Enabled by the Versatility of the Phenylselenonyl Group. *Chem. Eur. J.* **2016**, *22*, 18368−18372.
(26) Levchenko, T. I.; Kubel, C.; Najafabadi, B. K.; Boyle, P. D.; Cadogan, C.; Goncharova, L. V.; Garreau, A.; Lagugne-Labarthet, F.; Huang, Y. N.; Corrigan, J. F. Luminescent CdSe Superstructures: A Nanocluster Superlattice and a Nanoporous Crystal. *J. Am. Chem. Soc.* **2017**, *139*, 1129−1144.
(27) Evans, D. F. The determination of the paramagnetic susceptibility of substances in solution by nuclear magnetic resonance. *J. Chem. Soc.* **1959**, 2003.
(28) Zhao, Y.; Truhlar, D. The M06 suite of density functionals for main group thermochemistry, thermochemical kinetics, noncovalent interactions, excited states, and transition elements: two new functionals and systematic testing of four M06-class functionals and 12 other functionals. *Theor. Chem. Acc.* **2008**, *120*, 215−241.
(29) Hay, P. J.; Wadt, W. R. Ab initio effective core potentials for molecular calculations. Potentials for the transition metal atoms Sc to Hg. *J. Chem. Phys.* **1985**, *82*, 270−283.
(30) Wadt, W. R.; Hay, P. J. Ab initio effective core potentials for molecular calculations. Potentials for main group elements Na to Bi. *J. Chem. Phys.* **1985**, *82*, 284−298.
(31) Becke, A. D. Density-functional thermochemistry. III. The role of exact exchange. *J. Chem. Phys.* **1993**, *98*, 5648−5652.
(32) Chattopadhyay, S.; Deb, T.; Ma, H.; Petersen, J. L.; Young, V. G.; Jensen, M. P. Arylthiolate Coordination and Reactivity at Pseudotetrahedral Nickel(II) Centers: Modulation by Noncovalent Interactions. *Inorg. Chem.* **2008**, *47* (8), 3384−3392.
(33) Yang, L.; Powell, D. R.; Houser, R. P. Structural variation in copper(I) complexes with pyridylmethylamide ligands: structural analysis with a new four-coordinate geometry index, τ_4. *Dalton Trans.* **2007**, 955.
(34) Deb, T.; Anderson, C.; Chattopadhyay, S.; Ma, H.; Young, V. G.; Jensen, M. P. Steric and electronic effects on arylthiolate coordination in the pseudotetrahedral complexes [$(Tp^{Ph,Me})$Ni-SAr] ($Tp^{Ph,Me}$ = hydrotris{3-phenyl-5-methyl-1-pyrazolyl}borate). *Dalton Trans.* **2014**, *43*, 17489−17499.
(35) DuPont, J. A.; Yap, G. P. A.; Riordan, C. G. Influence of Ligand Electronic Effects on the Structure of Monovalent Cobalt Complexes. *Inorg. Chem.* **2008**, *47*, 10700−10707.
(36) Detrich, J. L.; Konecny, R.; Vetter, W. M.; Doren, D. J.; Rheingold, A. L.; Theopold, K. H. Structural Distortion of the TpCo-L Fragment (Tp = tris(pyrazolyl)borate). Analysis by X-ray Diffraction and Density Functional Theory. *J. Am. Chem. Soc.* **1996**, *118*, 1703−1712.
(37) Deb, T.; Anderson, C. M.; Ma, H. B.; Petersen, J. L.; Young, V. G.; Jensen, M. P. Scorpionato Halide Complexes [$(Tp^{Ph,Me})$Ni−X] [X = Cl, Br, I; $Tp^{Ph,Me}$ = Hydrotris(3-phenyl-5-methyl-1-pyrazolyl)-borate]: Structures, Spectroscopy, and Pyrazole Adducts. *Eur. J. Inorg. Chem.* **2015**, *2015*, 458−467.
(38) Abubekerov, M.; Gianetti, T. L.; Kunishita, A.; Arnold, J. Synthesis and characterization of coordinatively unsaturated nickel(II) and manganese(II) alkylcomplexes supported by the hydrotris(3-phenyl-5-methylpyrazolyl)borate ($Tp^{Ph,Me}$) ligand. *Dalton Trans.* **2013**, *42*, 10525−10532.
(39) Chattopadhyay, S.; Deb, T.; Petersen, J. L.; Young, V. G.; Jensen, M. P. Steric titration of arylthiolate coordination modes at pseudotetrahedral nickel(II) centers. *Inorg. Chem.* **2010**, *49*, 457−467.
(40) Green, W. L.; Sirianni, E. R.; Yap, G. P. A.; Riordan, C. G. Steric and electronic factor comparisons in hydrotris(3-phenylpyrazolyl)borate nickel(II) aryloxides. *Acta Crystallogr.* **2016**, *72*, 791−796.
(41) Deb, T.; Rohde, G. T.; Young, V. G.; Jensen, M. P. Aerobic and hydrolytic decomposition of pseudotetrahedral nickel phenolate complexes. *Inorg. Chem.* **2012**, *51*, 7257−7270.
(42) Chiou, T. W.; Liaw, W. F. Mononuclear Nickel(III) Complexes [$Ni^{III}(OR)(P(C_6H_3\text{-}3\text{-}SiMe_3\text{-}2\text{-}S)_3)]^-$ (R = Me, Ph) Containing the Terminal Alkoxide Ligand: Relevance to the Nickel Site of Oxidized-Form [NiFe] Hydrogenases. *Inorg. Chem.* **2008**, *47*, 7908−7913.
(43) Machonkin, T. E.; Boshart, M. D.; Schofield, J. A.; Rodriguez, M. M.; Grubel, K.; Rokhsana, D.; Brennessel, W. W.; Holland, P. L. Structural and spectroscopic characterization of iron(II), cobalt(II), and nickel(II) ortho-dihalophenolate complexes: insights into metal-halogen secondary bonding. *Inorg. Chem.* **2014**, *53*, 9837−9848.
(44) Chen, C. H.; Lee, G. H.; Liaw, W. F. Mononuclear [$Ni^{II}(L)(P(o\text{-}C_6H_4S)_2(o\text{-}C_6H_4SH))]^{0/1-}$ (L = Thiolate, Selenolate, PPh_3, and Cl) Complexes with Intramolecular [Ni···S···H···S]/[Ni···H···S] Interactions Modulated by the Coordinated Ligand L: Relevance to the [NiFe] Hydrogenases. *Inorg. Chem.* **2006**, *45*, 2307−2316.
(45) Darkwa, J. Cyclopentadienylnickel(II) Thiolato and Selenolato Complexes. Synthesis, Characterization, and X-ray Structure of (η^5-C_5H_5)Ni(SePh)(PPh_3). *Organometallics* **1994**, *13*, 3743−3745.
(46) Mautz, J.; Huttner, G. Reductive Activation of tripod Metal Compounds: Preparative Application. *Eur. J. Inorg. Chem.* **2008**, 1423−1434.
(47) Goldman, C. M.; Olmstead, M. M.; Mascharak, P. K. Discrete Mononuclear and Dinuclear Nickel(II) Complexes of Alkane- and Areneselenolates: Syntheses, Structures, and Properties of $(Et_4N)_2[Ni_2(Se(CH_2)_3Se)_3]$, $(Ph_4P)_2[Ni(SePh)_4]$, and $(Ph_4P)_2[Ni_2(\mu\text{-}2,4,6\text{-}(Me)_3C_6H_2Se)_2(2,4,6\text{-}(Me)_3C_6H_2Se)_4]\cdot 8CH_3CN$. *Inorg. Chem.* **1996**, *35*, 2752−2757.
(48) Melnick, J. G.; Parkin, G. Methyl and arylchalcogenolate complexes of cadmium in a sulfur rich coordination environment: syntheses and structural characterization of the tris(2-mercapto-1-tert-butylimidazolyl)hydroborato cadmium complexes [Tm^{But}]CdMe, and [Tm^{But}]CdEAr (E = O, S, Se, Te) and analysis of the bonding in chalcogenolate compounds. *Dalton Trans.* **2006**, 4207−4210.
(49) Melnick, J. G.; Docrat, A.; Parkin, G. Methyl, hydrochalcogenido, and phenylchalcogenolate complexes of zinc in a sulfur rich coordination environment: syntheses and structural characterization of the tris(2-mercapto-1-tert-butylimidazolyl)hydroboratozinc complexes [TmBut]ZnMe, [Tm^{But}]ZnEH (E = S, Se) and [Tm^{But}]-ZnEPh (E = O, S, Se, Te). *Chem. Commun.* **2004**, 2870−2871.
(50) Howard, W. A.; Trnka, T. M.; Parkin, G. Syntheses of the Phenylchalcogenolate Complexes (η^5-$C_5Me_5)_2Zr(EPh)_2$ (E = O, S, Se, Te) and (η^5-$C_5H_5)_2Zr(OPh)_2$: Structural Comparisons within a Series of Complexes Containing Zirconium-Chalcogen Single Bonds. *Inorg. Chem.* **1995**, *34*, 5900−5909.
(51) Hillier, A. C.; Liu, S. Y.; Sella, A.; Elsegood, M. R. J. Lanthanide Chalcogenolate Complexes: Synthesis and Crystal Structures of the Isoleptic Series [$Sm(Tp^{Me,Me})_2ER$] (E = O, S, Se, Te; $Tp^{Me,Me}$ = tris-3,5-Dimethylpyrazolylborate). *Inorg. Chem.* **2000**, *39*, 2635−2644.
(52) Marganian, C. A.; Vazir, H.; Baidya, N.; Olmstead, M. M.; Mascharak, P. K. Toward Functional Models of the Nickel Sites in [FeNi] and [FeNiSe] Hydrogenases: Syntheses, Structures, and Reactivities of Nickel(II) Complexes Containing [NiN3S2] and [NiN3Se2] Chromophores. *J. Am. Chem. Soc.* **1995**, *117*, 1584−1594.
(53) Hsieh, C. K.; Lo, F. C.; Lee, G. H.; Peng, S. M.; Liaw, W. F. Chelating and Tellurolate Ligand-Transfer Studies of the Complex fac-[$Fe(CO)_3(TePh)_3]^-$: Crystal Structures of Heterodinuclear $(CO)_3Mn(\mu\text{-}TePh)_3Fe(CO)_3$ and CpNi(TePh)(PPh_3). *J. Chin. Chem. Soc.* **2000**, *47*, 103−107.
(54) Schneider, J. J.; Kuhnigkh, J.; Kruger, C. Synthesis, characterization, X-ray structure and reactivity of the unbridged NiTe bond in [($\eta^5C_5H_5$)NiTe($C_6H_3Me_3)_2P(C_2H_5)_3$]. *Inorg. Chim. Acta* **1997**, *266*, 109−112.
(55) Menon, S. C.; Panda, A.; Singh, H. B.; Patel, R. P.; Kulshreshtha, S. K.; Darby, W. L.; Butcher, R. J. Tellurium azamacrocycles: Synthesis, characterization and coordination studies. *J. Organomet. Chem.* **2004**, *689*, 1452−1463.

https://doi.org/10.1021/acs.inorgchem.1c00066
Inorg. Chem. 2021, 60, 6327−6338

(56) Hsieh, C. H.; Hsu, I. J.; Lee, C. M.; Ke, S. C.; Wang, T. Y.; Lee, G. H.; Wang, Y.; Chen, J. M.; Lee, J. F.; Liaw, W. F. Nickel complexes of o-amidochalcogenophenolate(2-)/o-iminochalcogenobenzosemiquinonate(1-) pi-radical: synthesis, structures, electron spin resonance, and X-ray absorption spectroscopic evidence. *Inorg. Chem.* **2003**, *42* (12), 3925−3933.

(57) Gillespie, R. J. Bond Angles and the Spatial Correlation of Electrons. *J. Am. Chem. Soc.* **1960**, *82*, 5978−5983.

(58) Gorelsky, S. I.; Basumallick, L.; Vura-Weis, J.; Sarangi, R.; Hodgson, K. O.; Hedman, B.; Fujisawa, K.; Solomon, E. I. Spectroscopic and DFT Investigation of $[M\{HB(3,5\text{-}iPr_2pz)_3\}(SC_6F_5)]$ (M = Mn, Fe, Co, Ni, Cu, and Zn) Model Complexes: Periodic Trends in Metal−Thiolate Bonding. *Inorg. Chem.* **2005**, *44*, 4947−4960.

(59) Ming, L.-J. *Physical Methods in BioInorganic Chemistry: Spectroscopy and Magnetism*; University Science Books: Sausalito, CA, 2000.

(60) Drago, R. S.; Zink, J. I.; Richman, R. M.; Perry, W. D. Theory of isotropic shifts in the nmr of paramagnetic materials: Part II. *J. Chem. Educ.* **1974**, *51*, 464−467.

(61) Ram, M. S.; Riordan, C. G.; Ostrander, R.; Rheingold, A. L. Syntheses, Reactivity and Molecular Structures of *RSRS*-$[Ni(tmc)SC_6H_5](PF_6)$, *RRSS*-$[Ni(tmc)SC_6H_5](CF_3SO_3)$ and *RRSS*-$[Ni(tmc)](CF_3SO_3)$ (tmc = 1,4,8,11-Tetramethyl-1,4,8,11-tetraazacyclotetradecane). *Inorg. Chem.* **1995**, *34*, 5884−5892.

(62) Cho, J. H.; Yap, G. P. A.; Riordan, C. G. Structural, Spectroscopic, and Electrochemical Properties of a Series of High-Spin Thiolatonickel(II) Complexes. *Inorg. Chem.* **2007**, *46*, 11308−11315.

(63) Barbaro, P.; Bencini, A.; Bertini, I.; Briganti, F.; Midollini, S. The tetranuclear trianion $[Fe_4Te_4(SC_6H_5)_4]^{3-}$: crystal and molecular structure and magnetic properties. *J. Am. Chem. Soc.* **1990**, *112*, 7238−7246.

(64) Deb, T.; Jensen, M. P. Electrophilic Alkylation of Pseudotetrahedral Nickel(II) Arylthiolate Complexes. *Inorg. Chem.* **2015**, *54* (1), 87−96.

(65) Pearson, R. G.; Sobel, H.; Songstad, J. Nucleophilic reactivity constants toward methyl iodide and trans-dichlorodi(pyridine)-platinum(II). *J. Am. Chem. Soc.* **1968**, *90*, 319−326.

(66) Reich, H. J.; Hondal, R. J. Why Nature Chose Selenium. *ACS Chem. Biol.* **2016**, *11*, 821−841.

(67) Hansch, C.; Leo, A.; Taft, R. W. A survey of Hammett substituent constants and resonance and field parameters. *Chem. Rev.* **1991**, *91*, 165−195.

(68) Anslyn, E. V.; Dougherty, D. A. *Modern Physical Organic Chemistry*; University Science Books: Sausalito, CA, 2006.

(69) Zhang, J.; Adhikary, A.; King, K. M.; Krause, J. A.; Guan, H. R. Substituent effects on Ni−S bond dissociation energies and kinetic stability of nickel arylthiolate complexes supported by a bis(phosphinite)-based pincer ligand. *Dalton Trans.* **2012**, *41*, 7959−7968.

(70) Rombach, M.; Seebacher, J.; Ji, M.; Zhang, G. F.; He, G. S.; Ibrahim, M. M.; Benkmil, B.; Vahrenkamp, H. Thiolate Alkylation in Tripod Zinc Complexes: A Comparative Kinetic Study. *Inorg. Chem.* **2006**, *45*, 4571−4575.

(71) Picot, D.; Ohanessian, G.; Frison, G. The Alkylation Mechanism of Zinc-Bound Thiolates Depends upon the Zinc Ligands. *Inorg. Chem.* **2008**, *47*, 8167−8178.

https://doi.org/10.1021/acs.inorgchem.1c00066
Inorg. Chem. 2021, 60, 6327−6338